GSA Data Repository 2016314

Giant landslides and highstands of the Caspian Sea

Tomáš Pánek[1]*, Oliver Korup[2], Jozef Minár[3], Jan Hradecký[1]

1. Department of Physical Geography and Geoecology, Faculty of Science, University of Ostrava, Chittussiho 10, 710 00 Ostrava, Czech Republic
2. Institute of Earth and Environmental Sciences, University of Potsdam, Karl-Liebknecht-Str. 24, D-14476 Golm, Germany
3. Department of Physical Geography and Geoecology, Comenius University in Bratislava, Mlynská dolina, 842 15 Bratislava 4, Slovakia

*E-mail: tomas.panek@osu.cz

Summary: This data repository contains an inventory of the landslides in the Caspian Sea (Table DR1), results of AMS dating of shells from marine abrasion platforms cut across landslide toes (Table DR2), a description of the logistic regression method, as well as field photographs and cross sections that characterize the geomorphology and internal structures of selected landslide bodies (Figures DR1, DR2 & DR3).

Table DR 1: Inventory of landslides in the NE Caspian Sea basin.

Landslide No.	Latitude (°)	Longitude (°)	Landslide area (km^2)	Estimated volume (km^3)	Landslide length (km)	Landslide height (km)	H/L
1	46.75	57.47	1.33	0.05	1.17	0.16	0.14
2	46.74	57.48	0.54	0.02	0.54	0.11	0.20
3	46.74	57.49	0.14	0.00	0.5	0.09	0.19
4	46.73	57.52	0.17	0.00	0.56	0.07	0.13
5	46.65	57.51	1.92	0.07	1.55	0.15	0.10
6	46.65	57.50	0.89	0.03	1.12	0.15	0.13
7	46.67	57.41	4.91	0.17	1.43	0.17	0.12
8	46.46	57.46	0.57	0.02	0.67	0.12	0.18
9	46.44	57.42	0.98	0.03	0.7	0.12	0.17
10	46.53	55.76	3.64	0.13	2.6	0.17	0.07
11	46.53	55.73	2.51	0.09	1.82	0.17	0.09
12	46.55	55.71	13.94	0.49	5.05	0.19	0.04
13	46.55	55.65	0.21	0.00	0.5	0.07	0.15
14	46.55	55.64	1.92	0.07	1.95	0.19	0.09
15	46.54	55.60	7.18	0.25	2.32	0.19	0.08
16	46.54	55.51	1.68	0.06	2.09	0.18	0.09
17	46.52	55.49	5.25	0.18	2.17	0.18	0.08
18	46.50	55.47	13.02	0.46	4.52	0.19	0.04
19	46.48	55.50	0.55	0.02	0.74	0.11	0.15
20	46.48	55.49	0.57	0.02	0.94	0.15	0.15
21	46.45	55.44	1.64	0.06	1.71	0.18	0.10
22	46.45	55.42	2.40	0.08	1.84	0.19	0.10
23	46.44	55.40	7.68	0.27	3.38	0.19	0.06
24	46.42	55.38	2.78	0.10	1.79	0.18	0.10
25	46.39	55.38	20.78	0.73	5.9	0.20	0.03
26	46.35	55.38	10.07	0.35	2.5	0.20	0.08
27	46.32	55.39	3.52	0.12	2.77	0.19	0.07
28	46.31	55.40	0.54	0.02	0.64	0.14	0.21
29	46.30	55.40	0.88	0.03	1.03	0.15	0.15
30	46.29	55.40	0.29	0.01	0.85	0.14	0.17
31	46.29	55.40	1.02	0.04	1.35	0.16	0.11
32	46.28	55.40	0.53	0.02	0.93	0.14	0.15
33	46.28	55.40	0.50	0.02	0.95	0.14	0.15
34	46.27	55.41	0.09	0.00	0.43	0.08	0.19
35	46.27	55.42	1.13	0.04	1.5	0.15	0.10
36	46.27	55.42	0.31	0.01	0.68	0.12	0.18
37	46.29	56.22	7.13	0.25	3.2	0.16	0.05
38	46.27	56.22	0.13	0.00	0.37	0.07	0.20
39	46.24	56.17	2.13	0.07	2.23	0.15	0.07
40	46.23	56.16	5.02	0.18	3.02	0.15	0.05
41	46.21	56.14	0.54	0.02	0.83	0.07	0.08

42	46.22	56.14	1.60	0.06	1.53	0.11	0.07
43	46.16	56.21	0.17	0.00	0.44	0.07	0.17
44	46.15	56.21	0.47	0.01	0.6	0.10	0.17
45	46.14	56.20	0.37	0.01	0.79	0.11	0.13
46	46.14	56.20	0.08	0.00	0.34	0.08	0.23
47	46.13	56.20	0.67	0.02	0.73	0.11	0.15
48	46.13	56.21	0.50	0.01	0.47	0.10	0.21
49	46.06	56.16	0.20	0.00	0.64	0.11	0.17
50	46.06	56.18	0.20	0.00	0.57	0.11	0.18
51	46.05	56.19	0.05	0.00	0.35	0.07	0.20
52	46.06	56.19	0.04	0.00	0.3	0.07	0.24
53	46.05	56.19	0.02	0.00	0.17	0.02	0.14
54	46.05	56.18	0.06	0.00	0.43	0.09	0.21
55	46.05	56.20	0.10	0.00	0.41	0.07	0.16
56	46.05	56.20	0.15	0.00	0.56	0.08	0.13
57	46.08	55.58	0.58	0.02	0.57	0.08	0.13
61	46.01	55.21	1.87	0.07	1.89	0.15	0.08
62	46.02	55.20	0.54	0.02	0.65	0.10	0.16
63	46.00	55.22	1.24	0.04	1.75	0.15	0.09
64	45.99	55.27	2.04	0.07	2.3	0.14	0.06
65	45.98	55.28	2.47	0.09	2.75	0.14	0.05
66	45.97	55.28	3.51	0.12	2.61	0.15	0.06
67	45.95	55.29	1.70	0.06	1.21	0.13	0.11
68	45.95	55.31	0.50	0.01	0.6	0.10	0.16
69	45.94	55.32	1.46	0.05	1.76	0.12	0.07
70	45.93	55.34	2.36	0.08	1.97	0.13	0.06
71	45.92	55.36	0.13	0.00	0.43	0.09	0.21
72	45.91	55.37	0.15	0.00	0.54	0.09	0.16
73	45.92	55.37	0.03	0.00	0.3	0.07	0.22
74	45.91	55.40	0.16	0.00	0.45	0.08	0.18
75	45.90	55.41	0.65	0.02	0.63	0.10	0.16
76	45.90	55.42	0.12	0.00	0.35	0.07	0.20
77	45.89	55.43	0.12	0.00	0.42	0.06	0.15
78	45.86	55.43	0.28	0.01	0.43	0.09	0.20
79	45.83	55.47	0.04	0.00	0.29	0.04	0.13
80	45.91	55.24	0.41	0.01	0.55	0.08	0.14
81	45.93	55.18	1.17	0.04	1.3	0.09	0.07
82	45.98	55.13	0.64	0.02	1.07	0.13	0.13
83	45.96	55.11	2.43	0.09	1.94	0.16	0.08
84	45.98	55.12	1.67	0.06	2	0.16	0.08
85	45.95	55.09	2.93	0.10	2.5	0.16	0.06
86	45.96	55.11	0.11	0.00	0.38	0.06	0.17

87	45.95	55.11	0.06	0.00	0.38	0.07	0.18
88	45.95	55.11	0.09	0.00	0.44	0.07	0.16
89	45.91	55.04	7.29	0.26	3.72	0.19	0.05
90	45.90	55.05	1.25	0.04	1.54	0.15	0.10
91	45.88	55.04	7.36	0.26	3.32	0.19	0.06
92	45.94	55.07	8.94	0.31	3.72	0.17	0.05
93	45.93	55.04	3.58	0.13	3.61	0.18	0.05
94	45.92	55.05	0.53	0.02	1.19	0.17	0.14
95	45.86	55.09	15.46	0.54	5.4	0.19	0.04
96	45.84	55.09	0.81	0.03	1.06	0.08	0.08
97	45.80	55.17	3.13	0.11	2.88	0.17	0.06
99	45.83	55.15	3.08	0.11	1.4	0.13	0.09
100	45.84	55.12	2.74	0.10	1.15	0.12	0.10
101	45.79	55.17	1.46	0.05	2	0.16	0.08
102	45.78	55.18	1.74	0.06	1.9	0.16	0.09
103	45.77	55.18	5.61	0.20	3.82	0.19	0.05
104	45.77	55.20	0.12	0.00	0.42	0.11	0.25
105	45.77	55.20	0.11	0.00	0.49	0.11	0.23
106	45.76	55.21	5.03	0.18	2.96	0.18	0.06
107	45.75	55.22	2.84	0.10	3.17	0.18	0.06
108	45.75	55.23	2.43	0.08	2.32	0.17	0.07
109	45.74	55.25	3.05	0.11	2.14	0.17	0.08
110	45.73	55.26	3.68	0.13	3.4	0.18	0.05
111	45.74	55.28	0.60	0.02	1.16	0.13	0.11
112	45.72	55.28	2.14	0.07	3.03	0.18	0.06
113	45.73	55.30	2.49	0.09	1.71	0.16	0.09
114	45.74	55.31	0.67	0.02	1.2	0.13	0.11
115	45.75	55.32	0.37	0.01	0.46	0.08	0.17
116	45.75	55.33	0.37	0.01	0.61	0.11	0.18
117	45.74	55.34	1.69	0.06	1.65	0.14	0.09
118	45.73	55.35	1.96	0.07	1.4	0.16	0.11
119	45.72	55.37	0.09	0.00	0.45	0.10	0.21
120	45.72	55.37	0.32	0.01	0.69	0.12	0.18
121	45.72	55.37	1.99	0.07	2.19	0.16	0.07
122	45.71	55.38	2.81	0.10	2.72	0.17	0.06
123	45.70	55.40	4.35	0.15	3.22	0.18	0.06
124	45.69	55.41	2.83	0.10	2.66	0.19	0.07
125	45.69	55.41	1.86	0.07	2.21	0.18	0.08
126	45.68	55.43	4.39	0.15	3.08	0.19	0.06
127	45.66	55.44	6.48	0.23	2.4	0.19	0.08
128	45.64	55.44	0.42	0.01	1.55	0.17	0.11
129	45.64	55.44	0.37	0.01	1.21	0.15	0.13

130	45.64	55.44	0.31	0.01	0.8	0.15	0.19
131	45.63	55.44	2.58	0.09	2.81	0.17	0.06
132	45.61	55.44	8.68	0.30	3.76	0.18	0.05
133	45.59	55.44	4.68	0.16	2.82	0.17	0.06
134	45.57	55.42	15.00	0.52	3.98	0.17	0.04
135	45.54	55.41	0.80	0.03	1.45	0.14	0.10
136	45.54	55.39	3.72	0.13	2.5	0.17	0.07
137	45.53	55.37	2.09	0.07	1.48	0.16	0.11
138*	45.52	55.35	7.42	0.26	4.33	0.16	0.04
139	45.52	55.33	2.20	0.08	2.04	0.16	0.08
140	45.51	55.31	5.54	0.19	2.31	0.15	0.07
141	45.51	55.27	5.01	0.18	2.27	0.15	0.07
142	45.51	55.24	11.77	0.41	4.6	0.17	0.04
143*	45.49	55.21	6.76	0.24	3.8	0.16	0.04
144	45.48	55.21	1.96	0.07	1.86	0.15	0.08
145*	45.47	55.22	7.57	0.26	3.63	0.16	0.04
146	44.92	54.32	1.19	0.04	1.27	0.10	0.08
147	44.99	54.33	6.77	0.24	3.14	0.13	0.04
148	44.98	54.30	1.18	0.04	1	0.14	0.14
149	44.91	54.20	6.48	0.23	2.41	0.14	0.06
150	44.89	54.15	2.10	0.07	1.52	0.15	0.10
151	44.90	54.18	1.47	0.05	1.06	0.14	0.13
152	45.03	54.22	1.21	0.04	1.1	0.10	0.09
153	45.04	54.21	1.80	0.06	1.17	0.13	0.11
154	45.03	54.17	8.66	0.30	2.16	0.15	0.07
155	44.99	54.14	1.97	0.07	1.75	0.13	0.07
156	44.94	54.02	7.15	0.25	3.53	0.17	0.05
157	44.93	54.00	5.22	0.18	2.9	0.17	0.06
158	44.92	53.95	4.20	0.15	2.46	0.18	0.07
159	44.91	53.91	12.22	0.43	3.09	0.20	0.06
160	44.91	53.86	6.01	0.21	2.59	0.18	0.07
161	44.91	53.84	4.73	0.17	3.29	0.18	0.05
162	44.91	53.82	2.54	0.09	2.38	0.18	0.07
163	44.92	53.80	2.98	0.10	1.68	0.17	0.10
164	44.92	53.78	2.38	0.08	2.56	0.16	0.06
165	44.93	53.77	5.72	0.20	3.13	0.16	0.05
166	44.91	53.75	2.36	0.08	1.21	0.13	0.11
167	44.09	53.13	3.08	0.11	1.25	0.15	0.12
168	44.45	51.23	1.24	0.04	0.78	0.16	0.21
169	44.44	51.20	0.45	0.01	0.75	0.14	0.19
170	44.47	51.04	0.46	0.01	0.86	0.14	0.16
171	44.42	51.03	6.94	0.24	3	0.15	0.05

172	44.46	51.04	0.59	0.02	0.8	0.13	0.16
173	44.49	51.05	1.16	0.04	1.28	0.17	0.13
174	44.50	51.04	2.01	0.07	1.26	0.18	0.15
175	44.50	51.01	5.76	0.20	1.47	0.19	0.13
176	44.52	50.96	2.02	0.07	1.77	0.16	0.09
177	44.90	53.76	1.56	0.05	1.19	0.13	0.11
178	44.90	53.72	9.35	0.33	3.33	0.19	0.06
179	44.89	53.74	0.04	0.00	0.27	0.07	0.26
180	44.89	53.74	0.11	0.00	0.38	0.07	0.19
181	44.89	53.70	0.67	0.02	1.66	0.18	0.11
182	44.87	53.68	3.43	0.12	2.53	0.20	0.08
182a	44.88	53.69	1.10	0.04	1.43	0.17	0.12
183	44.86	53.67	0.12	0.00	0.49	0.09	0.19
184	44.86	53.68	0.43	0.01	0.73	0.13	0.18
185	44.86	53.65	5.27	0.18	3.1	0.20	0.07
186	44.85	53.64	3.14	0.11	2.78	0.20	0.07
187	44.83	53.63	6.05	0.21	3.14	0.21	0.07
188	44.81	53.63	1.06	0.04	1.34	0.16	0.12
189	44.82	53.63	0.53	0.02	1.07	0.16	0.15
190	44.77	53.61	1.63	0.06	1.58	0.17	0.11
191	44.79	53.62	0.84	0.03	1.15	0.16	0.14
192	44.73	53.59	23.01	0.81	4.23	0.22	0.05
193	44.68	53.58	7.19	0.25	3.31	0.21	0.06
194	44.66	53.57	6.31	0.22	3.17	0.22	0.07
195	44.65	53.56	1.14	0.04	1.81	0.18	0.10
196	44.64	53.54	10.23	0.36	4.15	0.22	0.05
197	44.62	53.52	2.97	0.10	2.89	0.22	0.08
198	44.61	53.51	13.26	0.46	4.5	0.23	0.05
199*	44.56	53.48	22.00	0.77	6.34	0.24	0.04
200	44.59	53.49	4.15	0.15	2.3	0.16	0.07
201	44.53	53.48	10.04	0.35	4.44	0.23	0.05
202	44.51	53.50	1.23	0.04	1.12	0.18	0.16
203	44.50	53.49	2.38	0.08	1.13	0.18	0.16
204*	44.50	53.46	6.43	0.22	4.6	0.22	0.05
205	44.49	53.45	5.52	0.19	4.16	0.22	0.05
206*	44.47	53.43	12.07	0.42	3.7	0.23	0.06
207	44.45	53.41	6.10	0.21	3.8	0.23	0.06
208*	44.43	53.39	14.06	0.49	6.1	0.25	0.04
209	44.42	53.38	1.88	0.07	2.33	0.20	0.08
210	44.41	53.37	7.82	0.27	3.53	0.23	0.07
211	44.38	53.36	14.14	0.50	4.65	0.25	0.05
212	44.35	53.35	7.73	0.27	3.81	0.23	0.06

213	44.36	53.34	0.97	0.03	1.42	0.14	0.10
214	44.33	53.36	2.45	0.09	1.89	0.20	0.11
215	44.31	53.36	11.41	0.40	4.5	0.21	0.05
216	44.30	53.40	6.26	0.22	1.8	0.18	0.10
217	44.29	53.43	0.77	0.03	0.81	0.14	0.17
218	44.30	53.46	3.62	0.13	1.5	0.13	0.08
219	44.28	53.38	3.74	0.13	2.93	0.19	0.06
220	44.27	53.37	1.36	0.05	1.61	0.17	0.10
221	44.25	53.24	11.62	0.41	4.04	0.22	0.05
222	44.22	53.18	12.25	0.43	5.75	0.26	0.05
223	44.23	53.19	0.85	0.03	1.41	0.18	0.13
224	44.25	53.19	7.19	0.25	3.1	0.24	0.08
225	44.27	53.21	4.08	0.14	3.63	0.22	0.06
226	44.26	53.20	3.73	0.13	2.8	0.24	0.08
227	44.20	53.15	10.10	0.35	4.22	0.27	0.06
228	44.18	53.13	2.61	0.09	2.48	0.27	0.11
229	44.19	53.14	0.89	0.03	1.58	0.25	0.16
230	44.29	53.26	9.95	0.35	4.63	0.21	0.05
231	44.27	53.32	18.57	0.65	5.8	0.19	0.03
232	44.25	53.37	2.82	0.10	1.6	0.18	0.11
233	44.23	53.38	3.17	0.11	1.39	0.15	0.10
234	44.22	53.37	1.89	0.07	1.23	0.12	0.10
235	44.23	53.32	4.00	0.14	2.7	0.15	0.05
236	44.24	53.36	4.27	0.15	1.94	0.16	0.08
237	44.53	50.96	0.19	0.00	0.57	0.10	0.18
238	44.53	50.93	0.04	0.00	0.22	0.06	0.26
239	44.53	50.93	0.08	0.00	0.5	0.09	0.18
240	44.54	50.93	2.29	0.08	1.3	0.15	0.11
241	44.53	50.95	1.16	0.04	1.3	0.13	0.10
242	44.55	50.94	0.53	0.02	0.86	0.13	0.15
243	44.55	50.95	0.84	0.03	1.24	0.15	0.12
244	44.57	50.92	10.90	0.38	3.34	0.18	0.05
245	44.59	50.90	0.45	0.01	0.84	0.14	0.17
246	44.60	50.88	3.46	0.12	2.04	0.18	0.09
247*	44.61	50.86	8.26	0.29	3.04	0.18	0.06
248*	44.62	50.82	9.85	0.34	4.6	0.17	0.04
249	44.60	50.79	3.00	0.11	1.48	0.16	0.11
250	44.60	50.77	0.86	0.03	1.4	0.15	0.11
251	44.60	50.75	1.31	0.05	1.18	0.17	0.14
252	44.60	50.74	2.49	0.09	1.8	0.16	0.09
253	44.60	50.72	3.02	0.11	2.13	0.16	0.07
254*	44.60	50.69	5.42	0.19	2.7	0.17	0.06

255	44.60	50.67	1.85	0.06	1.07	0.16	0.15
256	44.61	50.65	1.34	0.05	0.95	0.16	0.17
258	44.62	50.59	4.83	0.17	2.75	0.16	0.06
259	44.62	50.52	0.80	0.03	1.2	0.14	0.12
260	44.63	50.40	4.28	0.15	1.05	0.13	0.12
261	44.64	50.33	1.96	0.07	1.26	0.13	0.11
262	44.60	50.29	2.17	0.08	1.15	0.15	0.13
263	44.58	50.29	0.06	0.00	0.46	0.08	0.18
264	44.58	50.29	0.03	0.00	0.38	0.07	0.18
265	44.56	50.28	0.04	0.00	0.25	0.05	0.20
266	43.54	51.83	35.01	1.23	4	0.24	0.06
267	43.50	51.88	13.87	0.49	3.8	0.22	0.06
268	43.31	51.89	10.14	0.36	4.12	0.19	0.05
269	43.29	51.88	2.40	0.08	1.8	0.13	0.07
270	43.26	51.93	9.09	0.32	3.7	0.19	0.05
271	43.29	51.90	1.17	0.04	1.07	0.12	0.11
272	43.30	51.91	0.41	0.01	0.64	0.10	0.15
273	43.38	51.90	7.61	0.27	3.22	0.21	0.07
274	43.38	51.93	2.03	0.07	1.5	0.17	0.12
275	43.34	51.94	2.94	0.10	2.21	0.19	0.08
276	43.44	51.90	24.16	0.85	2.7	0.24	0.09
277	43.48	51.92	12.43	0.44	2.9	0.24	0.08
278	43.70	51.78	4.38	0.15	1.44	0.15	0.10
279	43.68	51.76	3.14	0.11	1.15	0.16	0.14
280	43.71	51.79	1.14	0.04	1.05	0.14	0.13
281	43.72	51.85	7.44	0.26	1.5	0.13	0.09
282	43.71	51.85	3.09	0.11	0.9	0.12	0.14
283	43.66	51.75	2.48	0.09	1.43	0.16	0.11
284	43.76	51.69	5.71	0.20	3.8	0.18	0.05
285	43.84	51.75	2.87	0.10	1	0.15	0.15
286	43.86	51.75	0.64	0.02	0.7	0.10	0.14
287	43.82	51.75	0.89	0.03	0.9	0.12	0.14
288	43.81	51.74	1.11	0.04	0.85	0.11	0.13
289	43.82	51.70	5.42	0.19	1.6	0.17	0.10
290	43.80	51.67	3.60	0.13	1.7	0.17	0.10
291	43.78	51.71	7.23	0.25	2.4	0.18	0.08
292	43.77	51.72	1.86	0.06	0.9	0.14	0.15
293	43.74	51.70	10.20	0.36	2.14	0.19	0.09
294	42.63	54.33	0.98	0.03	1.1	0.21	0.19
295	42.64	54.35	2.54	0.09	1.93	0.23	0.12
296	42.62	54.31	0.47	0.01	0.65	0.18	0.28
297	42.66	54.35	1.56	0.05	1.6	0.23	0.14

299	42.66	54.36	0.65	0.02	1.1	0.20	0.18
300	42.74	54.38	17.67	0.62	5.3	0.27	0.05
301	42.71	54.38	4.96	0.17	2.04	0.25	0.12
302	42.77	54.39	4.13	0.14	1.63	0.22	0.14
303	42.86	54.45	19.80	0.69	5.35	0.26	0.05
304	42.89	54.46	1.68	0.06	2.28	0.23	0.10
305	42.90	54.46	5.05	0.18	3.6	0.24	0.07
306	42.91	54.47	5.43	0.19	3.18	0.24	0.07
308	42.93	54.48	2.51	0.09	1.6	0.22	0.14
309	42.96	54.56	1.02	0.04	1.15	0.18	0.15
310	42.95	54.55	0.29	0.01	0.7	0.14	0.19
311	42.97	54.59	2.95	0.10	1.95	0.16	0.08
313	41.99	53.92	1.63	0.06	1.5	0.18	0.12
314	42.00	53.93	2.20	0.08	1.3	0.19	0.14
315	42.10	53.10	4.45	0.16	1.7	0.14	0.08
316	42.08	53.08	2.05	0.07	1.4	0.13	0.09
317	42.07	53.07	0.25	0.00	0.5	0.10	0.19
318	42.00	52.96	3.21	0.11	1.24	0.12	0.10
319	41.97	52.93	1.43	0.05	0.8	0.11	0.14
320	41.89	52.87	1.93	0.07	1.22	0.10	0.08
321	41.88	52.86	1.13	0.04	1	0.10	0.10
322	41.83	52.83	0.37	0.01	0.53	0.10	0.18
323	41.71	52.28	1.91	0.07	1.43	0.03	0.02
500	46.02	55.17	13.72	0.48	4.6	0.19	0.04
501	46.05	55.17	4.21	0.15	3.5	0.17	0.05
	46.0	55.1					0.0
502	7	7	8.00	0.28	3.9	0.17	4

*Landslide investigated in the field. Volumes were estimated by multiplying mean landslide thickness by its footprint area. Field inspection revealed that reasonable thickness estimates for landslides with areas >0.5 km^2 were ~35 m; smaller landslides with areas of 0.1-0.5 km^2 were about ~20 m thick on average, whereas the smallest (<0.1 km^2) were only ~10 m thick.

Table DR 2: Results of AMS radiocarbon dating of shells from marine abrasion platforms cut across landslide toes.

Sample ID[a] UGAMS#	Specimen	Landslide no.	Elevation of abrasion platform	Radiocarbon age [^{14}C yr BP]	δ^{13}C. ‰	Calendar age [cal yr BP](2σ)[b]
13560	*Dreissena sp.*	248	–23 m asl	350 ± 20	0.4	Out of range
13234	*Dreissena sp.*	248	–23 m asl	380 ± 20	0.4	Out of range
13233	*Dreissena sp.*	204	–12 m asl	12,350 ± 30	2.4	13,998–13,576
13554	*Didacna sp.*	138	–12 m asl	12,400 ± 35	1.7	14,057–13,646
13230	*Dreissena sp.*	208	0 m asl	12,450 ± 30	2.2	14,098–13,720
13232	*Dreissena sp.*	199	0 m asl	12,430 ± 30	2.0	14,082–13,694
13551	*Dreissena sp.*	145	0 m asl	11,910 ± 30	2.2	13,496–13,193
13558	*Dreissena sp.*	204	0 m asl	12,290 ± 35	1.7	13,922–13,502
13555	*Dreissena sp.*	208	+22 m asl	12,280 ± 35	2.4	13,909–13,493
13559	*Dreissena sp.*	204	+22 m asl	12,170 ± 35	1.5	13,794–13,409
13556	*Dreissena sp.*	199	+22 m asl	12,490 ± 35	1.9	14,133–13,758
13557	*Dreissena sp.*	199	+22 m asl	12,380 ± 35	2.5	14,037–13,616
13553	*Didacna sp.*	145	+50 m asl	39,420 ± 170	1.5	43,163–42,522

[a]Dated in the UGAMS laboratory, University of Georgia, Centre for Applied Isotope Studies, United States.

[b]Calibrated using dataset Marine13 (Reimer et al., 2013) by adding ΔR = 26 ± 69 (weighted mean of localized reservoir correction for the Caspian Sea; http://calib.qub.ac.uk/marine)

Methods: Bayesian robust logistic regression

We compared the geometries of the Caspian Sea landslides with a global sample of mainly large (>10^6 m3) 591 terrestrial and 81 submarine landslides that we compiled from the literature (Korup, 2012). We conducted a Bayesian robust logistic regression (Kruschke, 2011) using the mobility index *H*/*L* and log-transformed landslide volume $\log_{10}V$ as predictors. Logistic regression assigns membership probabilities to each of the Caspian landslides, and helps to decide whether they belong more likely to either the terrestrial or marine domain. Contrary to its name, logistic regression is a method for classifying, and in its Bayesian form allows specifying all uncertainties in the model that arise from the data:

$$\mu_p = sig(b_0 + b_1 x_1 b_2 x_2 + \ldots + b_n x_n), \quad (1)$$

where μ_p is the mean expected value of the response variable, in this case, the probability of belonging either to the terrestrial or submarine landslide class; and b_i are the regression coefficients for the i data vectors containing the predictor variables x_i, respectively; $sig(x)$ is the sigmoid function defined as

$$sig(x) = 1/(1 + e^{-x}) \quad (2)$$

The modeled outcome y is nominal, and can be either 0 (= terrestrial) or 1 (= submarine), and has a Bernoulli distribution as its likelihood function:

$$y = dbern(\mu) \quad (3)$$

We combined Equations (1) to (3) to learn credible models from the data. We adopted a Bayesian approach that allows estimating the full posterior probability distributions of each regression parameter (instead of only their means) from the data. We used equal-sized random subsets of the terrestrial and submarine data to reduce potential bias from classifying data that are unbalanced and dominated by one of the two classes.

The model setup is hierarchical. The first level of the model contains the combined Equations (1) to (3), whereas the second level of hierarchy contains the parameters describing the probability distributions of the regression coefficients b_i; the second-level parameters are called hyperpriors. Our model assumes that the regression intercept b_0 is normally distributed as $\mathcal{N}(0, 10^{12})$, where $\mathcal{N}(\mu, \sigma^2)$ is the normal distribution with mean μ and variance σ^2. The model further assumes that the coefficients b_1 (for *H*/*L*), and b_2 (log-transformed landslide volume) come from *t*-distributions each with normally distributed means from $\mathcal{N}(0{,}10)$, and gamma-distributed variances from $\Gamma(10^{-4}, 10^4)$. The degrees of freedom of these *t*-

distributions were sampled from a custom function $1 - Glog(1 - U(0,1))$, where $U(0,1)$ is the uniform distribution, and $G = 1$ is a gain parameter (see Kruschke, 2011, for more details). We chose a low gain parameter to better highlight possible interactions between the two predictors *H*/*L* and $\log_{10}V$. While the assumption of a normal distribution of the intercept b_0 is consistent with the central limit theorem in probability theory, the use of *t*-distributions for b_1 and b_2 emphasizes the tails of the normal distribution. The net effect is that regression coefficients with values near zero will lower the variance in the *t*-distribution, hence producing more accurate estimates of the regression coefficients. Using *t*-distributions instead of normal distributions thus ensures a higher robustness against outliers when estimating the posterior distributions of the regression coefficients.

We implemented the model in the open-source programming environment *R* using the *rjags* library (Kruschke, 2011), which uses a numerical Markov Chain Monte Carlo sampling scheme to compute the posterior distributions of all regression coefficients based on standardized input data. We took into account only coefficient values b_i that were credibly different from zero, i.e. whose posterior distributions did not contain zero in their 95% highest density interval, which is the Bayesian analog to the 95% confidence interval in frequentist statistics. We tested various combinations of parameter values for the different hyperpriors, but found that, given the large amount of data points, our posterior distributions remained largely robust irrespective of the exact choices of hyperpriors. In other words, our initial beliefs about the distribution of the regression parameters are more heavily weighted and adjusted by the high number of data points and hence the likelihoods (instead of the prior beliefs), so that slight changes in the hyperpriors do not noticeably change the shape and location of the posterior distributions.

Figure DR1: Geomorphic features of selected landslides in the NE Caspian Depression from cross sections and photos that are characteristic of the landslide bodies (M l – Miocene limestones; P+M – Paleogene and Miocene claystones, marls and chalk).

Cross section of landslide no. 248 Dzhigalgan (Mangyshlak peninsula) together with panels A-D showing surface features. A: Headscarp of Holocene landslide deposit nested within older landslide body; detachment area covered by dunes (landslide no. 247). B: 30- to 40-m high headscarp of Holocene landslide; proximal blocks of Miocene limestones indicate rotational failure. C: Central part of landslide body with large blocks and debris cover marine cliff at +50 m asl, related to Early Khvalynian highstand of the Caspian Sea. D: Large limestone blocks (see person for scale) were abraded by wave action during the formation of wave-cut platform at –23 m asl.

Cross section of landslide no. 254 (Mangyshlak peninsula) together with panels E-H showing geomorphic features of heavily eroded landslide deposit. A marine abrasion platform and cliff at +50 m asl truncate this landslide body. E: Amphitheatre-shaped source area of landslide covered by climbing dunes. F: Landslide headscarp and detachment zone covered by ~5-10 m of aeolian deposits. Only the largest rotated limestone blocks in the foreground rise above the otherwise smoothed landslide body. G: Abrasion platform and cliff at +50 m asl associated with the Early Khvalynian transgression. H: 20-m high abrasion cliff cutting across the landslide toe.

Cross section of landslide no. 204 (Sor Kaydak area) together with panels I-L showing geomorphic features of landslide deposit that has been heavily altered by wave action and gully erosion. Only a portion of the original deposit survived the transgressive phases following the Early Khvalynian. I: Thick aeolian deposits nearly bury the smoothed landslide scarp. J: Gullies incised into landslide body. K: Pronounced abrasion platforms related to the Early Khvalynian (+50 m asl) and Late Khvalynian (0 m asl) transgressions cut into the landslide toe. L: Distal section of landslide exposes contact between Paleogene claystones capped by thin veneer of partly eroded landslide debris.

Cross section of landslide no. 208 (Sor Kaydak area) together with panels M-P showing one of the largest identified landslides in the Caspian Sea region. The landslide toe is heavily trimmed, whereas the landslide body is distinctly beveled of its original hummocky topography below +50 m asl following Middle to Late Khvalynian and Holocene highstands of the Caspian Sea. M: 40- to 50-m high headscarp incised by gully. N: Hummocky topography of the landslide source area revealing rotational movement (view from the headscarp). O: Beveled distal section of the landslide (+20 m asl). P: 20- to 30-m high marine cliff in distal part of the landslide mark erosion of sea-level highstands, Sor Kaydak salt marsh.

Figure DR1

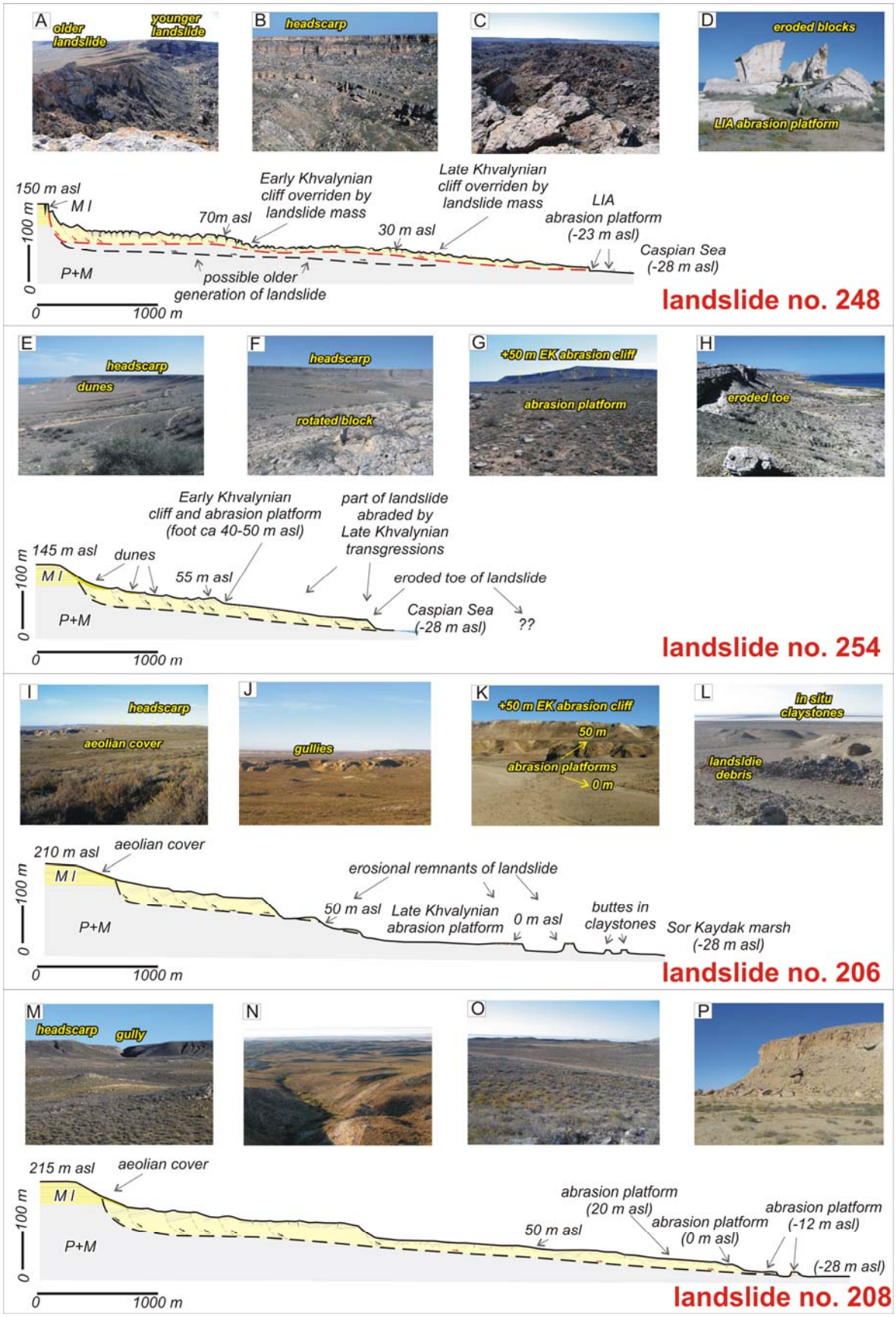
A
older landslide
younger landslide
B
headscarp
C
D
eroded blocks
LIA abrasion platform
150 m asl
M I
100 m
0
P+M
70m asl
Early Khvalynian cliff overriden by landslide mass
30 m asl
Late Khvalynian cliff overriden by landslide mass
LIA abrasion platform (-23 m asl)
Caspian Sea (-28 m asl)
possible older generation of landslide
0
1000 m
landslide no. 248
E
headscarp
dunes
F
headscarp
rotated block
G
+50 m EK abrasion cliff
abrasion platform
H
eroded toe
Early Khvalynian cliff and abrasion platform (foot ca 40-50 m asl)
part of landslide abraded by Late Khvalynian transgressions
145 m asl
dunes
M I
100 m
0
P+M
55 m asl
eroded toe of landslide
Caspian Sea (-28 m asl)
??
0
1000 m
landslide no. 254
I
headscarp
aeolian cover
J
gullies
K
+50 m EK abrasion cliff
50 m
abrasion platforms
0 m
L
in situ claystones
landsldie debris
210 m asl
aeolian cover
M I
100 m
0
P+M
erosional remnants of landslide
50 m asl
Late Khvalynian abrasion platform
0 m asl
buttes in claystones
Sor Kaydak marsh (-28 m asl)
0
1000 m
landslide no. 206
M
headscarp
gully
N
O
P
215 m asl
aeolian cover
M I
100 m
0
P+M
abrasion platform (20 m asl)
50 m asl
abrasion platform (0 m asl)
abrasion platform (-12 m asl)
(-28 m asl)
0
1000 m
landslide no. 208

Figure DR2: Internal structure of selected landslide deposits featuring gravitational deformations that resemble tectonic structures. Original bedrock bedding is nearly horizontal throughout the study area.

A: Large tilted block of competent Miocene limestone embedded within landslide debris, central part of landslide no. 145, Beyneu region. B: Gravitationally folded and faulted, deformable claystones near large limestone block in (A). C: Rotated block of rigid Miocene limestone bed and adjacent (D) compression structures in plastic claystones. E: Contact between competent Miocene limestone blocks deformed predominantly by brittle fractures, and (F) highly sheared and fragmented Paleogene-Miocene claystones, mudstones, and marls. Note completely mixed landslide debris with rigid limestone blocks floating in folded chalk layers, and pervasively fragmented and sheared claystones, marls, and mudstone units, central part of landslide no. 199, Sor Kaydak region. G: Pop-up structure in limestones near compressional toe of landslide no. 254, Mangyshlak peninsula. H: Recumbent fold in bed of fragmented Miocene limestone, central part of landslide no. 199, Sor Kaydak region. I: Exposure within toe of landslide no. 208, Sor Kaydak region, indicates multiple reactivations with alternating gravitational thrust sheets (separating two claystone bands marked B1 and B2) and diamict bed (A); note pronounced shear zones between B1 and B2. J: Exposure of the toe of landslide no. 208 with minor asymmetric folds in shear band between displaced block A1 and in situ sedimentary units B1 and B2. Note how brownish claystone B1 is partly dragged into the shear band. K: Compressional structures within less competent Miocene limestones (thin bedded strata) in central part of landslide no. 208. L: Superimposed shear zones in Paleogene claystones of distal part of landslide no. 145, Beyneu region. M: Minor fold in the thrust-like shear band in distal part of landslide no. 145.

Figure DR2

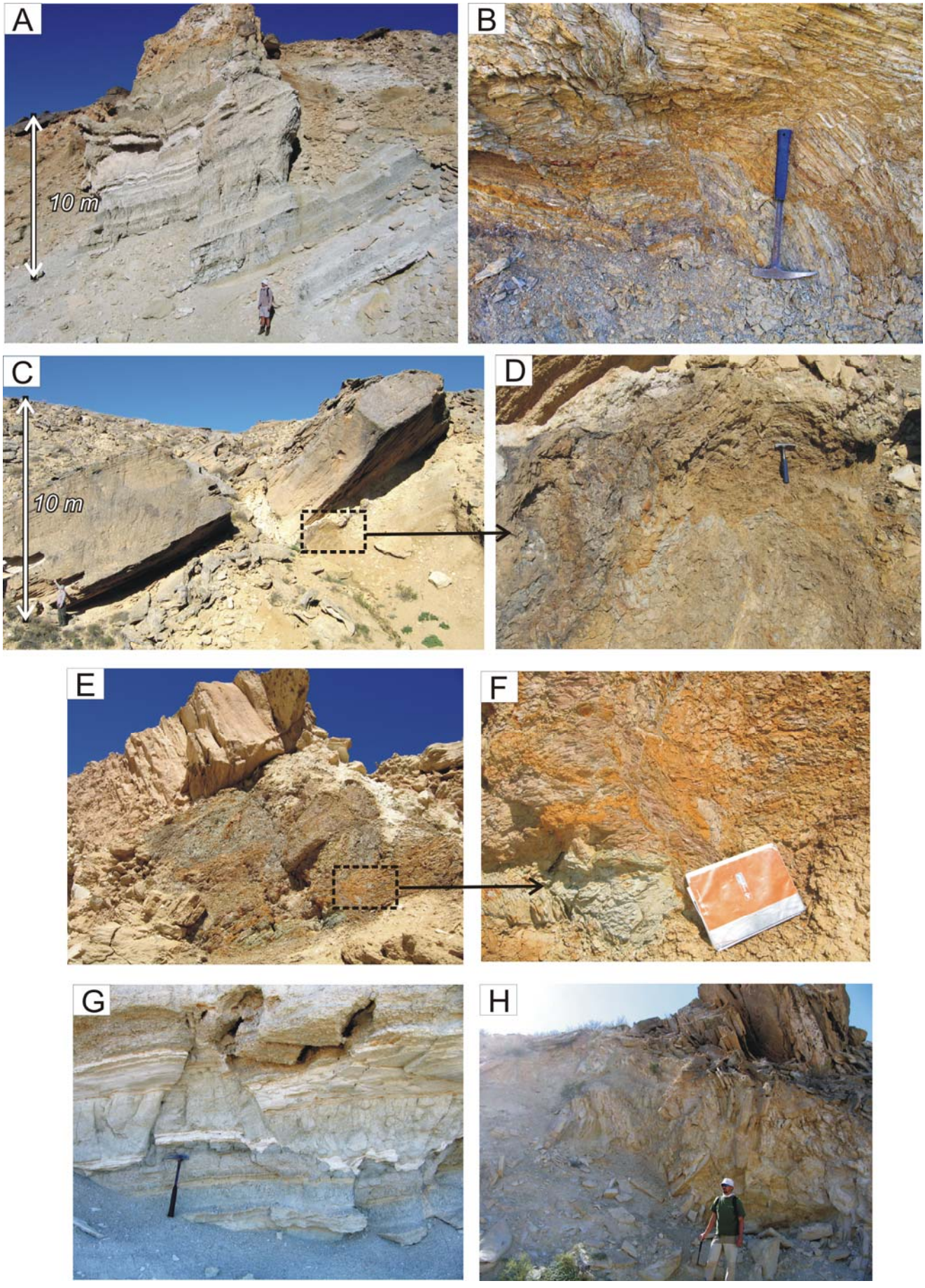

Figure DR2 (continued)

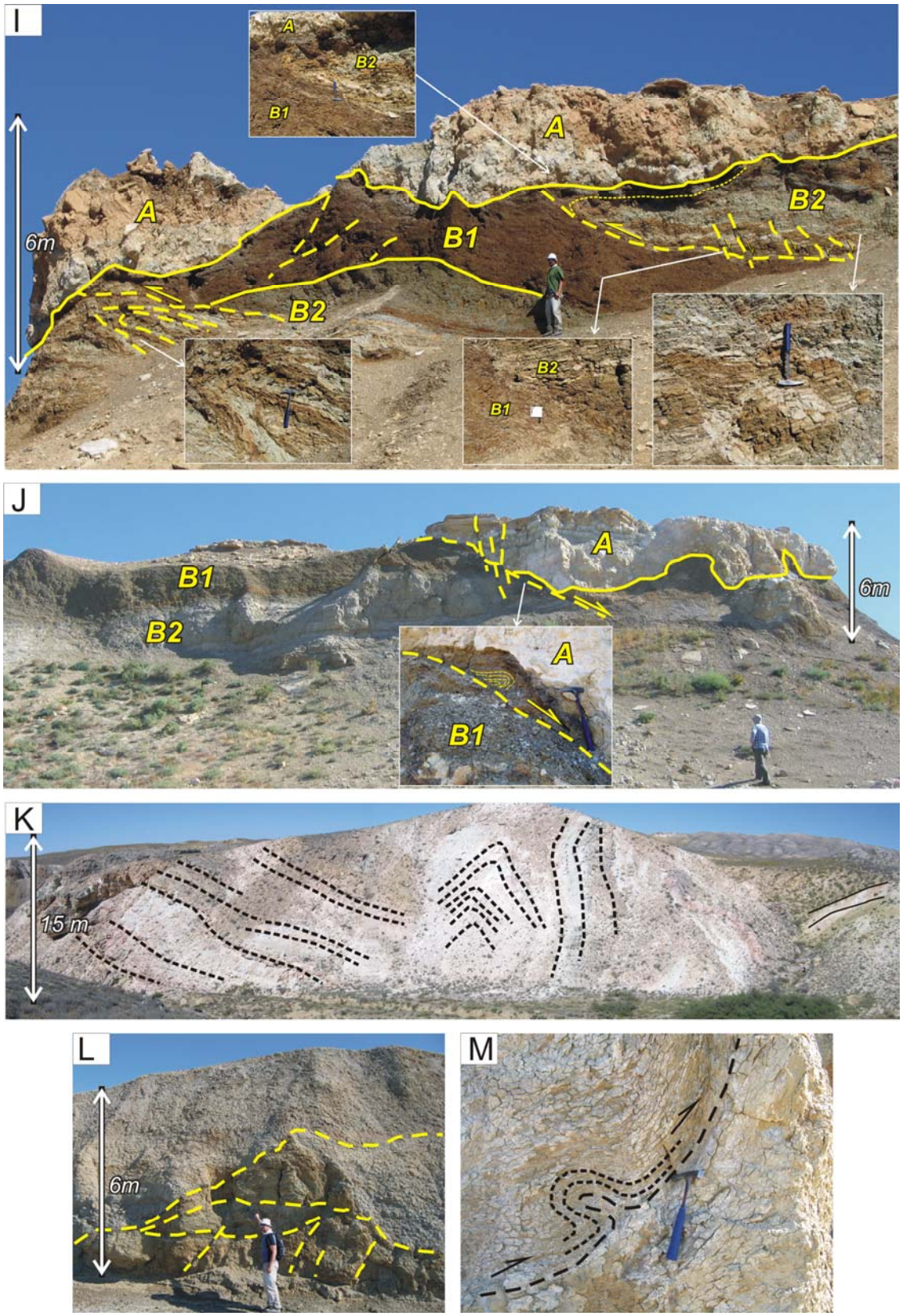

Figure DR3: Geomorphic markers on landslide bodies that help determine minimum age of slope failure and erosion.

A: Early Khvalynian cliff (+50 m asl) cut across landslide no. 254, Mangyshlak peninsula. B: The same cliff at landslide no. 143, Beyneu region. C: Abrasion platform at 0 m asl (Late Khvalynian highstand) cutting across deformed landslide deposit no. 247, Mangyshlak peninsula. D: Extensive abrasion platform (+22 m asl; Late Khvalynian transgression) with abundant shells of *Dreissena and Didacna sp.* dated to 13,794–13,409 cal. yr B.P., central part of landslide no. 199, Sor Kaydak region. E: Pronounced abrasion platform at 0 m asl (Late Khvalynian transgression) truncating distal part of landslide no. 208, Sor Kaydak region. *Dreissena sp.* shells from this location returned an age of 14,098–13,720 cal. yr B.P. Note reactivated landslide no. 209 in the background. F and G: Abraded remnants of the toe of landslide no. 208 with distinct beach levels (see beach and near-shore pebble facies in inset in (G), and abrasion platforms at –12 m asl (Late Khvalynian transgression) covered by *Dreissena sp.* shells with age of 13,998 – 13,576 cal. yr B.P. H: Climbing aeolian dunes in the detachment zone of landslide no. 138, Sor Kaydak region; photo taken from the 30-m high headscarp. I: Abrasion platform and cliff (–23 m asl), where embedded *Dreissena sp.* shells gave an uncalibrated age 350 ± 20 and 380 ± 20 ^{14}C BP, which is beyond the range of the Marine13 calibration curve.

Figure DR3

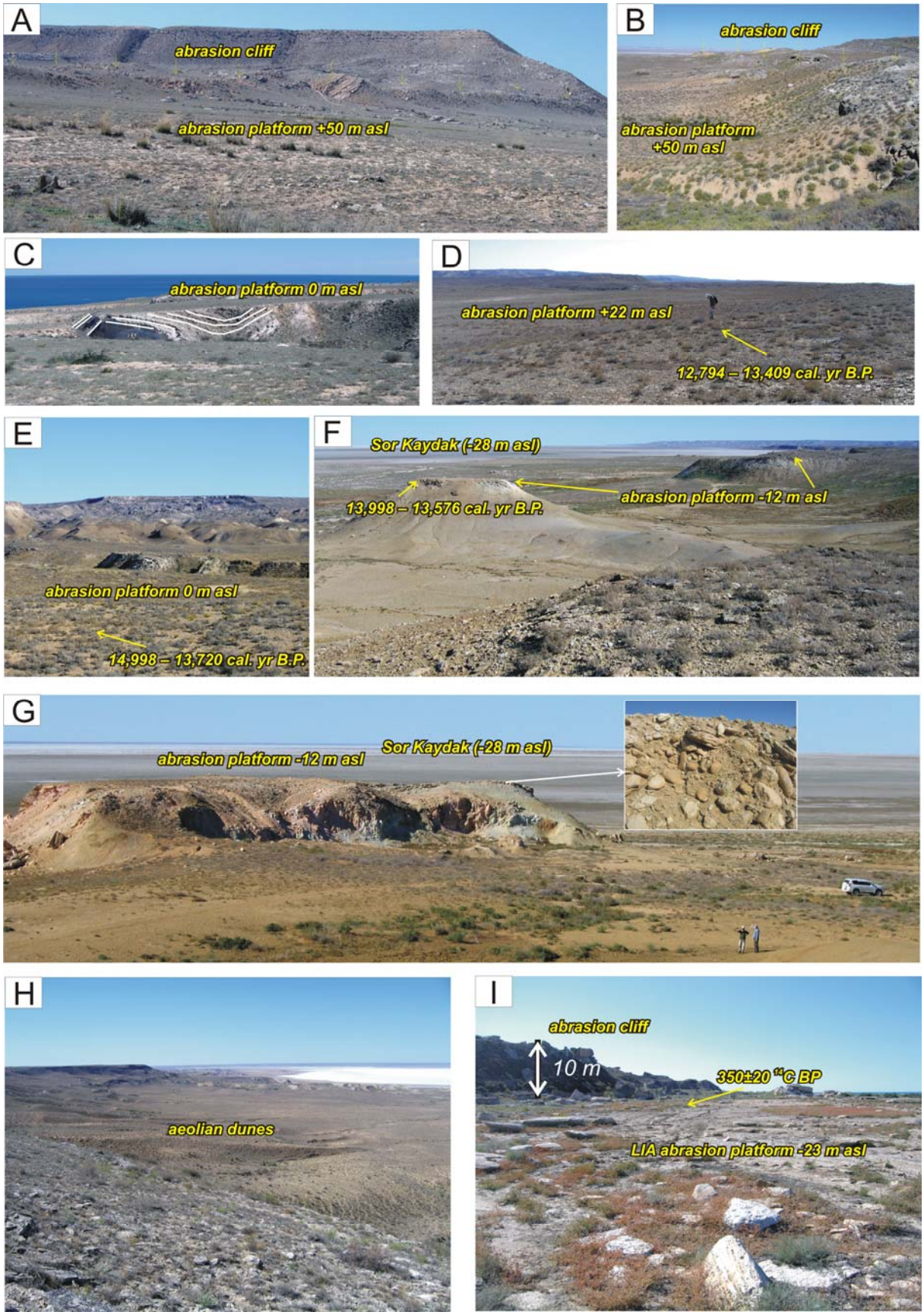
A
abrasion cliff
abrasion platform +50 m asl
B
abrasion cliff
abrasion platform
+50 m asl
C
abrasion platform 0 m asl
D
abrasion platform +22 m asl
12,794 – 13,409 cal. yr B.P.
E
abrasion platform 0 m asl
14,998 – 13,720 cal. yr B.P.
F
Sor Kaydak (-28 m asl)
13,998 – 13,576 cal. yr B.P.
abrasion platform -12 m asl
G
abrasion platform -12 m asl
Sor Kaydak (-28 m asl)
H
aeolian dunes
I
abrasion cliff
10 m
350±20 ¹⁴C BP
LIA abrasion platform -23 m asl

ADDITIONAL REFERENCES CITED

Korup, O., 2012. Earth's portfolio of extreme sediment transport events. Earth-Science Reviews, v. 112, p. 115–125.

Kruschke, J.K., 2011, Doing Bayesian Data Analysis, Academic Press, Burlington, 653pp.

Reimer, P.J., Bard, E., Bayliss, A., Beck, J.W., Blackwell, P.G., Bronk Ramsey, C., et al., 2013. IntCal13 andMarine13 radiocarbon age calibration curves 0–50,000 years cal BP. Radiocarbon v. 55, p. 1869–1887.